



Original Article

Design and 3D printing of adjustable modulus porous structures for customized diabetic foot insoles



Zheng Ma ^{a, b}, Jiacheng Lin ^{a, b}, Xiaoyue Xu ^{a, b}, Ziwei Ma ^{a, b}, Lei Tang ^{a, b},
Changning Sun ^{a, b}, Dichen Li ^{a, b}, Chaozong Liu ^c, Yongming Zhong ^d, Ling Wang ^{a, b, *}

^a State Key Laboratory for Manufacturing Systems Engineering, Xi'an Jiaotong University, 710054, Xi'an, Shaanxi, China

^b School of Mechanical Engineering, Xi'an Jiaotong University, 710054, Xi'an, Shaanxi, China

^c John Scale Centre for Biomedical Engineering, University College London, Royal National Orthopaedic Hospital, Stanmore, HA74LP, Hong Kong

^d Shandong Weigao Pharmaceutical Co., Limited. No.20 Xingshan Road, Hi-tech District, Weihai, Shandong, China

ARTICLE INFO

Article history:

Received 2 June 2018

Received in revised form

22 October 2018

Accepted 22 October 2018

Available online 26 October 2018

Keywords:

Adjustable gradient modulus

Porous structures

Diabetic insoles

3D printing

ABSTRACT

Designs with adjustable gradient modulus have become necessary for applications with special demands such as diabetic insole, in which the contact stress between the foot and insole is a critical factor for ulcers development. However, since the adjustment of elastic modulus on certain regions of insole can hardly be achieved via materials selection, a porous structural unit with varying porosity becomes a feasible way. Therefore, porous structural units associated with adjustable effective modulus and porosity can be employed to construct such insoles by 3D printing manufacturing technology. This paper presents a study on the porous structural units in terms of the geometrical parameters, porosity, and their correlations with the effective modulus. To achieve this goal, finite element analyses were carried out on porous structural units, and mechanical tests were carried out on the 3D printed samples for validation purposes. In this case, the mathematical relationships between the effective modulus and the key geometrical parameters were derived and subsequently employed in the construction of an insole model. This study provides a generalized foundation of porous structural design and adjustable gradient modulus in application of diabetic insole, which can be equally applied to other designs with similar demands.

© 2018 The Authors. Production and hosting by Elsevier B.V. on behalf of KeAi Communications Co., Ltd. This is an open access article under the CC BY-NC-ND license (<http://creativecommons.org/licenses/by-nc-nd/4.0/>).

1. Introduction

Nowadays, designs with adjustable gradient modulus has become necessary for applications with special demands such as diabetic insole since the contact stress between foot and insole is a critical factor for ulcer development [1–3]. It has been found that the symptoms of diabetic foot are significantly alleviated by reducing and uniformly distributing plantar pressure, which can be achieved by the customized insole with extra metatarsal dome and arch support [4–6]. Therefore, different regions of insoles should be assigned with different modulus for localized support. Traditional methods, such as molding and machining, are only applicable to

manufacture insoles with homogeneous mechanical property, which hinders the effectiveness of insoles for slowing down the development of ulcers [7]. Besides, such insoles are relatively high-cost due to the demanding requirements of selecting materials and relatively long designing and manufacturing period, which is hard to afford for the majority of patients [3,7]. Since the adjustment of modulus can hardly be achieved by materials selection, a porous structure with adjustable mechanical properties (effective modulus) becomes a feasible way.

3D printing techniques are now widely used for the freedom of manufacturing materials with complex geometry [8–10], which makes them capable of manufacturing porous structural units for customized diabetic insoles. Among all kinds of 3D printing techniques, the material extrusion technique (MEX) is the most commonly used technique due to its low cost in instruments and materials, which makes it a fairly good candidate for fabrication [11]. Nevertheless, common flexible materials, like thermoplastic polyurethane (TPU) and thermoplastic elastomer (TPE), have effective moduli that are beyond the demand of alleviating plantar

* Corresponding author. State Key Laboratory for Manufacturing Systems Engineering, Xi'an Jiaotong University, 710054, Xi'an, Shaanxi, China.

E-mail address: menlwang@xjtu.edu.cn (L. Wang).

Peer review under responsibility of Editorial Board of International Journal of Lightweight Materials and Manufacture.

pressure [4,7,12]. In this case, porous structural units were utilized to yield lower effective modulus with flexible, MEX-supported materials as desired.

Many researchers have been working on the manufacturing of customized diabetic insoles with 3D printing techniques. Miguel et al. presented a CAD methodology to design and manufacture therapeutic insoles by MEX. Feasibility of this methodology was verified both practically and economically by several prototypes in their latest paper [13]. Telfer et al. enrolled twenty participants in the comparison of 3D-printed insoles and subtractive milled insoles. Results show that the use of 3D-printed insoles yields lower peak pressures in 88% of the plantar regions of interests [14]. Though many studies have provided feasible methods in this field, few of them focusing on porous structural units (size, geometric parameter, porosity and effective modulus). Therefore, it's necessary to provide a general methodology of studying porous structural units, in order to map customized diabetic insoles and other possible applications.

To achieve this goal, a typical porous structural unit was selected. Based on this porous structural unit, a FE model was constructed to calculate its effective modulus [15]. The feasibility of FE model was validated by carrying out compressive tests on the 3D-printed porous structures. Then both compressive tests and FEA simulations were employed to measure the effective modulus of the porous structure. For further analyses in mechanical properties, orthogonal experiments were carried out to determine geometric parameters that are sensitive to the effective modulus of units. When the sensitive geometric parameters were determined, further study was carried out to obtain the mathematical relationships between the sensitive parameters and the effective modulus of porous structural units. Meanwhile, mathematical relationships between porosity and geometric parameters were also presented.

2. Materials and methods

2.1. Preparation of porous structural units

Initially, porous structural units were designed by parametric modeling. Among all units, the ellipsoidal structural unit (Fig. 1(a)) was employed in this study because of its relatively satisfying 3D-printing quality and resilience under compression. By adjusting the geometric parameters, it can achieve a wide range of effective elastic modulus, which is necessary for customized diabetic insoles. In the construction of ellipsoidal structural units, geometric parameters were determined based on the character of ellipsoidal structure ('A', the length of long axis of ellipsoidal cross section. 'B', the length of short axis of ellipsoidal cross section. 'T', the thickness of wall of the hollow ellipsoid. 'H', the thickness of plate between layers). The side lengths of units vary from 4.4 mm to 8.1 mm and the heights of units vary from 3.3 mm to 5.1 mm. The porosity of units is in the range of 30.91%–46.97%. For the convenience of

printing and compressive tests, samples were arrayed of $5 \times 5 \times 5$ replications of a single unit as Fig. 1 (b). Several printed samples are shown as Fig. 1(c).

2.2. Manufacturing porous structures with MEX

The desktop MEX printer used in this study is 3DP-300B (Shaanxi Hengtong Intelligent Machine Co., Ltd.). The printing precision is 0.4 mm. Slicing files were generated in Cura 15.04 (Ultimaker, Netherlands). Printing settings were as fellow: nozzle temperature of 235 °C, nozzle diameter of 0.4 mm, layer thickness of 0.2 mm, printing speed of 30 mm/min, and filling rate of 100%. TPE filament (eLastic, Shenzhen Esun Industrial Co., Ltd) with diameter of $1.75 \text{ mm} \pm 0.05 \text{ mm}$ was used in this study.

2.3. Compressive test

Compressive tests were conducted with electromechanical universal testing machine (ETM103A from Shenzhen Wance Testing Machine Co.). During compression, samples were compressed at a constant speed of 1 mm/min, with a sampling frequency of 120 Hz. Tests were terminated when the force reached the upper limitation of 200 N, in order to keep the samples within linear elastic range and avoid plastic deformation or internal structure interference. Three samples ($N = 3$) were tested for each group, and the average value was determined. Average length of each sample was measured with caliper. The experimental effective elastic modulus of the samples can be obtained from the slop of stress–strain curves, which is expressed in Eq. (1).

The equation [16] employed in effective modulus calculation:

$$E = \frac{F}{A} \cdot \frac{h}{\Delta h} = k\# \quad (1)$$

where F is the external loading, A is the nominal cross-sectional area, h is the original height, Δh is the compressive displacement and k is the slope of the elastic range in the stress–strain curve.

2.4. Finite element analysis (FEA)

Compression testing simulations of various porous structure models were carried out via FEA method in ABAQUS 6.14–4 (Dassault, France), as shown in Fig. 2. Models were created in SolidWorks 2017 SP4.0 (Dassault, France) and converted into IGES format before imported into ABAQUS. Each porous structural unit was free-meshed by tetrahedral element with an approximate global size of 2 mm [17]. According to the simulation of ordinary walking [12], the stresses of plantar were within the linear elastic range of TPE material. Therefore, the material in FEA model can be considered as an elastomer with two key factors, Young's modulus and Poisson ratio. According to the compression testing standard ASTM D695 [18], solid cylinders with diameter of 12.7 mm, height

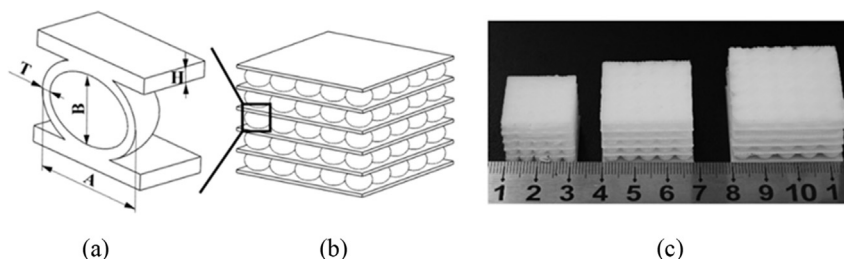


Fig. 1. (a) Cutaway view of ellipsoidal structural unit; (b) Sketch of arrayed samples ($5 \times 5 \times 5$); (c) MEX printed TPE samples.

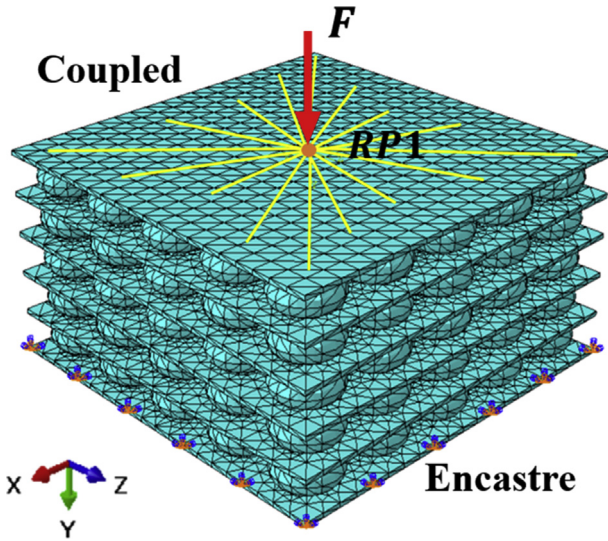


Fig. 2. FE model set-up as representative of the effective model of the porous structural units.

of 25.4 mm were printed under the printing settings listed above, in order to determine the mechanical property of TPE material. After calculation, the Young's modulus of TPE is 14.525 MPa and Poisson's ration is 0.3.

To authentically simulate the compressive tests, the boundary and loading conditions of the FE model were consistent with those applied in the compressive tests [12,15]. Since the base of the porous structural unit was fully constrained for any degree of freedom during the compressive test, the boundary condition of the bottom layer was set up accordingly as fully constrained (Encastre) for the FE model. The surface of the porous structural unit was coupled with the reference point (RP1) that is located at the center. An axial compressive load of 200N, perpendicular to the surface, was applied via RP1. Thus, every point on the surface was under the same compressive load as RP-1, which is equal to a uniformly distributed load of 200N over the surface. Finally, the general compressive displacement that was parallel to the load was calculated. With the results of deforming displacement, the effective modulus of porous structural units was calculated by Eq. (1).

2.5. Orthogonal experiments

In order to find out the sensitive factors that could have dominating influence on mechanical properties, orthogonal experiments were carried out at first. Based on the guidelines for orthogonal experiments [19,20], four factors (wall thickness 'T', long axis 'A', short axis 'B' and plate thickness 'H') were chosen as geometrical parameters from the cutaway view in Fig. 1(a). And 3 levels were set for each factor, as shown in Table 1. Orthogonal experiments were arranged according to L9 (3^4).

Table 1 Level settings in orthogonal experiments (wall thickness 'T', long axis 'A', short axis 'B' and plate thickness 'H').

Factors	Levels		
	1	2	3
T/mm	0.4	0.6	0.8
A/mm	3.5	4.5	5.5
B/mm	2.5	3	3.5
H/mm	0.4	0.6	0.8

All samples were printed using the mentioned printing settings and effective modulus was determined from both the compressive tests and the FEA simulations. By gathering and analyzing all testing results, the level of sensitivity of each factor was determined by the range, calculated from Eqs. (2)–(4).

The dominating equations [19] are listed below (i, j = 1,2,3)

$$I_{ij} = \sum_{j=1}^3 \text{the value of factor } i \text{ level } j\# \tag{2}$$

$$K_{ij} = \frac{I_{ij}}{\text{repetition of level } i\#} \tag{3}$$

$$R_i = \max(K_{i,1}, K_{i,2}, K_{i,3}) - \min(K_{i,1}, K_{i,2}, K_{i,3})\# \tag{4}$$

where I_{ij} denotes the estimating value for the level j of factor i; K_{ij} represents the overall mean value for the level j of factor i; R_i stands for the range of overall mean value for factor i.

2.6. Parametrical study

Based on the previous tests, two of the most effective factors, wall thickness 'T' and long axis 'A', were chosen as the sensitive factors in the following study, and their effects were investigated thoroughly in sequential manner. The range of 'T' was set from 0.4 mm to 0.9 mm at an interval of 0.1 mm to generate six wall thickness sequential models; likewise, the range of 'A' was set from 3.5 mm to 6.5 mm at an interval of 0.5 mm to generate 7 long axis sequential models. All generated models were printed out under the same printing settings and were put into mechanical testes to determine the effective modulus.

3. Results

Mechanical tests and FEA simulations were conducted according to the design of orthogonal experiment and parametrical study. Typical result of one instance with the largest deformation is presented in Fig. 3(a) as a comparison between the mechanical test and FEA simulation. Displacement nephogram of FEA model under ultimate load condition is expressed in Fig. 3(b). The original height of sample (h) is 17.4 mm. The compressive displacement of compressive test (Δh) is 4.95 mm and the compressive displacement of FEA simulation ($\Delta h'$) is 5.81 mm. Fairly good agreement has been achieved in both methods in terms of the maximum displacement.

The effective modulus of FEA simulations and compression tests for orthogonal models are compared in Table 2. Calculated from Eqs. (2)–(4), the range of each factor from two methods was determined and portrayed in Fig. 4. As indicated in the diagram, the order of sensitivity for the four factors was: wall thickness 'T' > long axis 'A' > plate thickness 'H' > short axis 'B'. The optimized result [19] associated with the smallest effective modulus was determined as well. Orthogonal model No.10 denotes the optimized model set-up (A = 5.5 mm, B = 3 mm, T = 0.4 mm, H = 0.4 mm).

From the contrasts between two methods' results of orthogonal models, results can be summarized that: 1) These two sensitivity sequences of ellipsoidal models' parameters in descending order are completely identical. 2) Orthogonal model No.10 has been proved to possess the smallest effective modulus among all orthogonal series models via FEA simulation or compressive test.

Based on the conclusion of orthogonal experiments, two geometric parameters, wall thickness 'T' and long axis 'A', were chosen to conduct parametrical study. Stress–strain curves of 'T' sequential

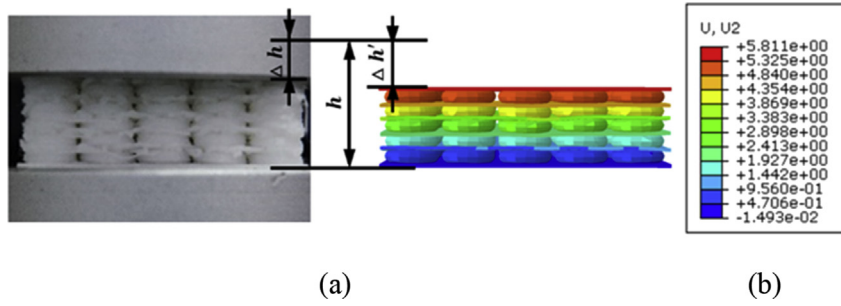


Fig. 3. (a) Contrasts between compressive tests and FEM simulations; (b) Displacement nephogram under ultimate load condition.

Table 2
Effective modulus results of FEA simulations and compression tests of orthogonal models.

	1	2	3	4	5	6	7	8	9	10
Effective modulus from compressive tests	1.964 ± 0.16	0.782 ± 0.06	0.489 ± 0.04	3.975 ± 0.33	2.472 ± 0.18	1.483 ± 0.11	5.768 ± 0.41	4.216 ± 0.35	2.261 ± 0.13	0.427 ± 0.03
Effective modulus from FEA	1.083	0.511	0.342	2.204	1.101	0.759	3.684	2.779	1.449	0.275

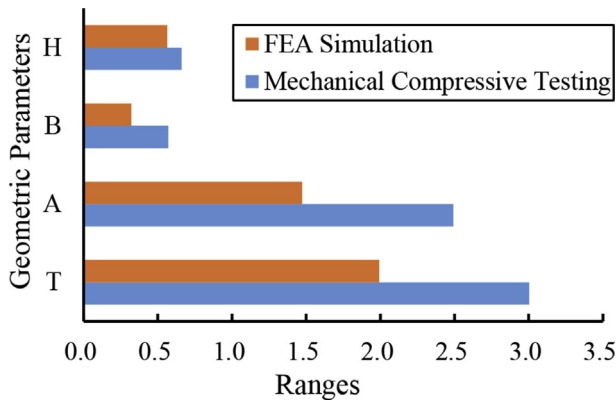


Fig. 4. Factor ranges in orthogonal experiments. (Plate thickness 'H'; Short axis 'B'; Long axis 'A'; Wall thickness 'T').

models are shown in Fig. 5(a). Images of samples under different strain conditions in compression are expressed in Fig. 5(b).

After data fitting, the mathematical relationships between wall thickness and effective modulus were obtained, as shown in Fig. 6(a). In the same way, the effect of the long axis A was also investigated in Fig. 6(b). Porosity for various parametrical model

was also determined and correlated to the effective modulus, as presented in Fig. 7(a) and Fig. 7(b).

4. Discussion

In this study, a FE model was developed to study the mechanical properties of porous structural units. Mesh convergence study was carried out first to guarantee the accuracy in FE calculation [15]. Since it is a static process, time integration is irrelevant to the result. Focus should be paid on the meshing size. In the analysis, the approximate global size ranges from 0.5 mm to 3.0 mm with an interval of 0.5 mm. Relative errors of these six groups are less than 5%. Because the proper setting of meshing size is determined by the trade-off between accuracy and time span, the approximate global size of 2.0 mm is a feasible option.

Compressive tests and FEA simulations were conducted in parallel, in order to correlate the porous structural design to the effective modulus. Overall, the effective moduli determined from the FEA simulation vary from 0.27 MPa to 3.68 MPa, which are 40.5% ± 10.3% lower than those derived from compressive tests. This may be due to the following reasons: 1) The actual Young's modulus of TPE material is higher than the value that was assigned in FE model for the material property. As mentioned in 2.4, the effective modulus of solid cylinder is used to represent the Young's

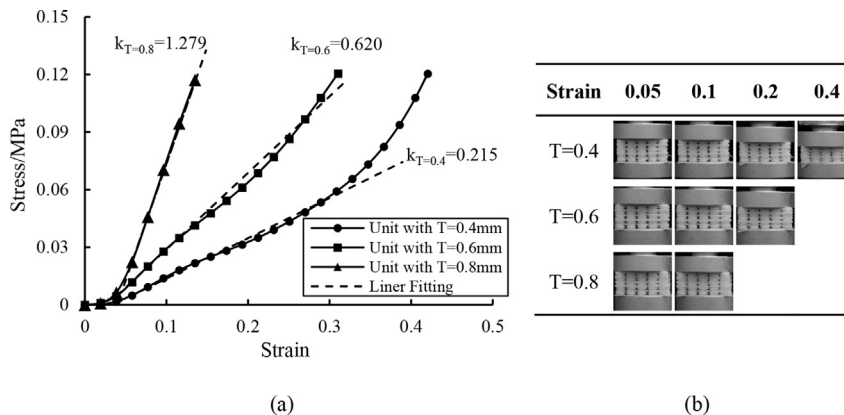


Fig. 5. (a) Stress –strain curves of 'T' sequential models; (b) Images of the ellipsoidal models under different strain conditions.

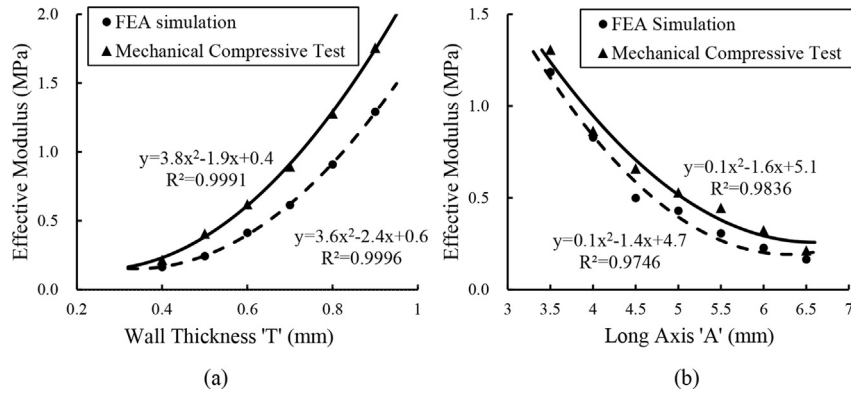


Fig. 6. (a) The mathematical relationship between wall thickness 'T' and effective modulus ('T' is changeable while other parameters are A = 6.5 mm, B = 3 mm, H = 0.5 mm); (b) The mathematical relationship between long axis 'A' and effective modulus ('A' is changeable while other parameters are T = 0.4 mm, B = 3 mm, H = 0.5 mm).

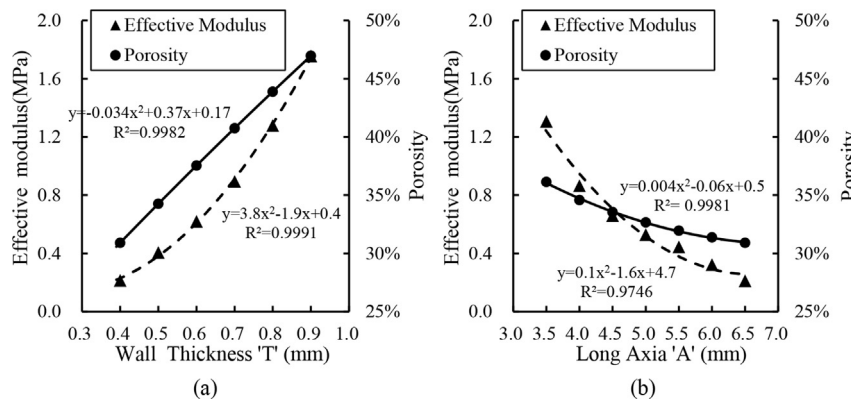


Fig. 7. (a) The mathematical relationships between wall thickness 'T' and mechanical properties (porosity and effective modulus). (b) The mathematical relationships between long axis 'A' and mechanical properties (porosity and effective modulus).

modulus in FE model. Confined by the principle of MEX [11,21–23], however, the solid cylinder is not an ideal one with 0% porosity and it may yield a lower modulus than the material itself. 2) Interference inside the porous structural unit occurs in the compressive test. As the load increases, the internal structures (Fig. 1(b)) gradually expand and touch the surroundings [23,24]. Then the internal structures pile up, resulting in a larger cross sectional area and therefore a higher effective modulus. While in FEA model, the interference is not considered because of its algorithm. 3) Confined by the MEX, fracture, cracks and other flaws are inevitable in the printed samples. These flaws are not possible to be replicated in the FEA model [25]. 4) The constrains in the FEA model are not identical to the compressive test. An ideal encastre as in the FEA model (Fig. 2) is impossible in practice. It needs to be noted that 3) and 4) can only prove a mismatch between the compressive tests and FEA simulations. Whether the results of FEA simulations are lower than those from compressive tests or not has not been strongly proved by 3) and 4) yet. Whatsoever, the tendencies shown by FEA simulations are in accordance with those of mechanical testing, which indicates that FEA can still be a very good candidate for parametrical optimization at fairly low cost and more convenience.

As the orthogonal experiment shows, wall thickness 'T' and long axis 'A' are among the most sensitive factor to the effective modulus of porous structural unit while short axis 'B' and plate thickness 'H' impose relatively rare influence on its mechanical property. Several reasons contribute to this conclusion: 1) Wall thickness 'T' can significantly affect the effective sectional area in porous structural units. The increase in wall thickness will

generate more area within porous structural units to bear the load, which consequently yields a bigger effective modulus [26]. 2) Wall thickness is closely related with the printing quality via MEX technique. Since TPE material is flexible and sticky during the depositing process, porous structural units with thin wall (less than one or two times of the diameter of nozzle) are susceptible to the crack or flaw while porous structural units with thick wall (more than two times of the diameter of nozzle) are more tolerant [22]. 3) Mechanical properties of spherical or ellipsoid structure are remarkable influenced by eccentricity. By increasing the long axis 'A', the porous structural units will become flatter and decentralize the pressure concentration, which indirectly reduces the effective modulus and form a softer unit. 4) Since the external load was applied uniformly on the surface plate, the internal plate, instead of bearing load, just transmits the load internally to the lower part. Therefore, the plate thickness "H" has little effect on the stress distribution, which makes it rather irrelevant compared with the other two parameters like the wall thickness "T" and the long axis "A". In summary, geometric parameters that affect the effective sectional area and the internal stress distribution will significantly affect the effective modulus as well.

In addition to the instruction of porous structural design, the orthogonal experiment also provides an optimized porous structural unit with low effective modulus, the orthogonal model No.10. Since porous structural units were employed to reduce the effective modulus of material to satisfy the demand of mapping diabetic foot insoles [12,13,15], the orthogonal model No.10 is one of the best option.

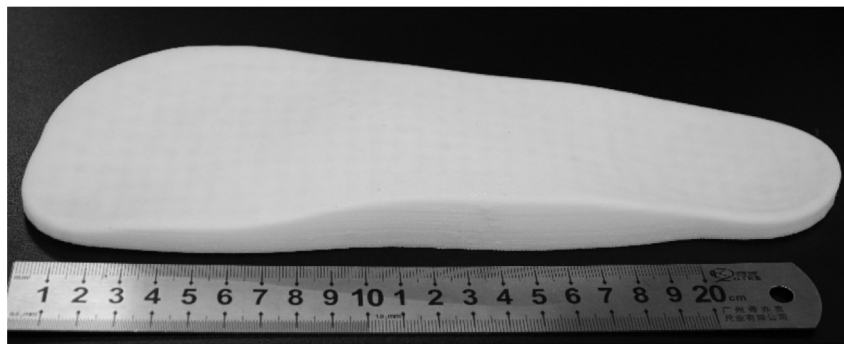
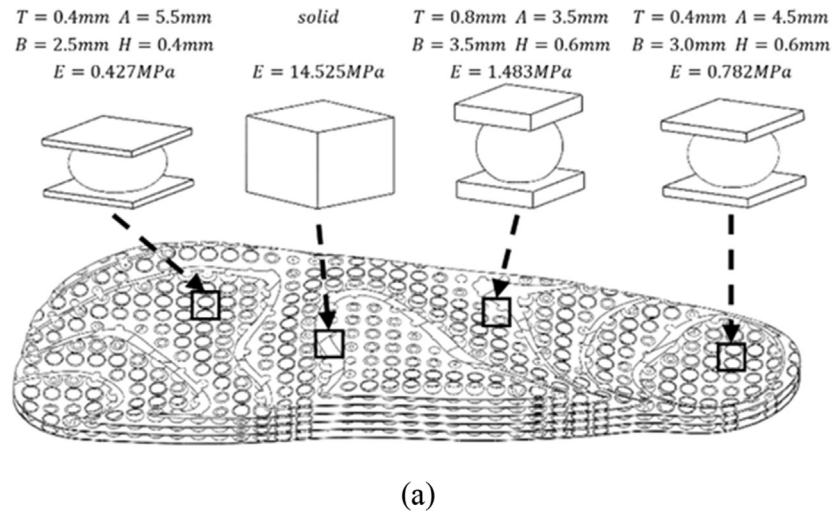


Fig. 8. (a) Diagram of filling customized diabetic foot insoles (without the coverage of external sphere); (b) Diagram of manufactured customized diabetic foot insole (with the coverage of external sphere).

In parametrical study, mathematical relationships between effective modulus and key geometric parameters were constructed from both the FEA simulations and compressive tests. Practical applications of mathematical relationships are listed as follow. 1) The range of effective modulus for the porous structure units was determined, varying from 0.21 MPa to 1.76 MPa, which meets the demand of reducing effective modulus to construct diabetic foot insoles [4,12,15]. 2) The mathematical relationships could be nested in a database, which is used to predict the effective modulus when geometric parameters are known or to generate geometric parameters when certain effective modulus is required. 3) Porosity is also an essential indicator of the density and effective modulus when compared with other porous structural units.

Focusing on the property of ellipsoidal porous structural units, evaluation could be summarized. 1) The elliptical unit possesses flexibility in adjusting its geometric size as well as its effective modulus, which enables this porous structural unit to satisfy both geometric and mechanical demands of designing the diabetic insoles or other possible applications 2) The ellipsoidal unit could remain its linear elasticity under normal plantar stress conditions [12], as shown in the stress–strain curves of sequential models. For this reason, this porous structural unit possesses a stable mechanical property as an elastomer. 3) The yield strength of ellipsoidal unit is far beyond the maximum pressure which merely

several times of normal plantar stress [4,12]. With the increase of load, the internal structures pile up and the effective modulus increases, like the latter range of stress–strain curves in Fig. 5(a). It is reasonable to assume that if the load keeps increasing, the effective modulus will increase along with it until it reaches the threshold of the material strength of TPE.

This study provides a generalized foundation of porous structural design for adjustable gradient modulus in application of diabetic insole, which can be equally applicable to other designs with similar demands. In the future, emphasis will be put on establishing database about the mechanical properties and key geometric parameters of porous structural units. Next, customized diabetic Fig. 8(a) [27].

The cost of one pair of insole is 27 US dollars approximately, which includes expenses on materials (7\$), equipment depreciation and maintenance (10\$), labor (10\$) etc. The cost is a lot less than the commercially available products in the market (80–100 dollars), which indicates good marketing opportunity of such a technique in the application of diabetic insole manufacturing.

The major limitation of this study is that only single type of structural unit was studied. Further study should expand the choices of other structural units in order to provide more flexibility of low modulus structural design, which will be suitable for a wider range of application.

5. Conclusion

This study presents a study on the porous structural units in terms of the geometrical parameters and their correlation with the porosity as well as the effective mechanical properties. Finite element analyses were carried out on porous structural units, and mechanical tests were carried out on the 3D printed samples for validation purposes. The mathematical relationships between the effective modulus and the key geometrical parameters were derived and subsequently employed in the construction of an insole model. This study also provides a generalized foundation of porous structural design for adjustable gradient modulus in application of diabetic insole, which can be equally applicable to other designs with similar demands.

Acknowledgements

The work was supported by the National Key R&D Program of China [2018YFB1107000] and the Key Program of international cooperation in Shaanxi Province [grant number 2017KW-ZD-02].

References

- [1] J.J. Van Netten, K. Bakker, J. Apelqvist, B.A. Lipsky, N.C. Schaper, The 2015 guidance of the international working group on the diabetic foot, *EWMA J.* 16 (1) (2016).
- [2] S. Bus, D. Armstrong, R. Deursen, J. Lewis, C. Caravaggi, P. Cavanagh, IWGDF guidance on footwear and offloading interventions to prevent and heal foot ulcers in patients with diabetes, *Diabetes Metabol. Res. Rev.* 32 (S1) (2016) 25–36.
- [3] N. Schaper, J. Van Netten, J. Apelqvist, B. Lipsky, K. Bakker, I. W. G. O. T. D. Foot, Prevention and management of foot problems in diabetes: a summary guidance for daily practice 2015, based on the IWGDF guidance documents, *Diabetes Metabol. Res. Rev.* 32 (2016) 7–15.
- [4] R. Waaijman, M. De Haart, M.L. Arts, D. Wever, A.J. Verlouw, F. Nollet, et al., Risk factors for plantar foot ulcer recurrence in neuropathic diabetic patients, *Diabetes Care* 37 (6) (2014) 1697–1705.
- [5] N. Guldemond, P. Leffers, N. Schaper, A. Sanders, F. Nieman, P. Willems, et al., The effects of insole configurations on forefoot plantar pressure and walking convenience in diabetic patients with neuropathic feet, *Clin. BioMech.* 22 (1) (2007) 81–87.
- [6] S.A. Bus, J.S. Ulbrecht, P.R. Cavanagh, Pressure relief and load redistribution by custom-made insoles in diabetic patients with neuropathy and foot deformity, *Clin. BioMech.* 19 (6) (2004) 629–638.
- [7] L. Begg, J. Burns, A comparison of insole materials on plantar pressure and comfort in the neuroischaemic diabetic foot, *Clin. BioMech.* 23 (5) (2008) 710–711.
- [8] D. Li, J. He, X. Tian, Y. Liu, A. Zhang, Q. Lian, et al., Additive manufacturing: integrated fabrication of macro/microstructures, *Jixie Gongcheng Xuebao (Chin. J. Mech. Eng.)* 49 (6) (2013) 129–135.
- [9] B. Lu, D. Li, X. Tian, Development trends in additive manufacturing and 3D printing, *Engineering* 1 (1) (2015) 85–89.
- [10] M. Qin, Y. Liu, J. He, L. Wang, Q. Lian, D. Li, et al., Application of digital design and three-dimensional printing technique on individualized medical treatment, *Zhongguo xiu fu chong jian wai ke za zhi= Zhongguo xiu fu chongjian waik e zazhi= Chin. J. Repar. Reconstr. Surg.* 28 (3) (2014) 286–291.
- [11] X.H. Zhang, L.C. Zhang, L.I. Zhi, Y.S. Shi, Rapid prototyping study of flexible materials based on fused deposition modeling, *J. Netshape Form. Eng.* 5 (2015) 81–85.
- [12] S. Jacob, M. Patil, Stress analysis in three-dimensional foot models of normal and diabetic neuropathy, *Front. Med. Biol. Eng.* 9 (3) (1999) 211–227.
- [13] M. Davia-Aracil, J.J. Hinojo-Pérez, A. Jimeno-Morenila, H. Mora-Mora, 3D printing of functional anatomical insoles, *Comput. Ind.* 95 (2018) 38–53.
- [14] S. Telfer, J. Woodburn, A. Collier, P. Cavanagh, Virtually optimized insoles for offloading the diabetic foot: a randomized crossover study, *J. Biomech.* 60 (2017) 157–161.
- [15] A. Ghassemi, A. Mossayebi, N. Jamshidi, R. Naemi, M. Karimi, Manufacturing and finite element assessment of a novel pressure reducing insole for Diabetic Neuropathic patients, *Australas. Phys. Eng. Sci. Med.* 38 (1) (2015) 63–70.
- [16] P.P. Benham, R.J. Crawford, C.G. Armstrong, *Mechanics of engineering materials*, Longman Harlow, Burnt Hill, Harlow Essex CM20 2JE, England, England Longman Scientific & Technical, 1996, pp. 64–81.
- [17] S.C. Tadepalli, A. Erdemir, P.R. Cavanagh, Comparison of hexahedral and tetrahedral elements in finite element analysis of the foot and footwear, *J. Biomech.* 44 (12) (2011) 2337–2343.
- [18] American Society for Testing and Materials, Standard test methods of compression testing of metallic materials at room temperature, 1990 Annual Book of ASTM Standards, ASTM, West Conshohocken, PA, 1990, pp. 98–105.
- [19] D. Bo, *The statistic method of testing data analysis*, Tsinghua University Press, Beijing, 1995, pp. 203–212.
- [20] A.S. Hedayat, N.J.A. Sloane, J. Stufken, *Orthogonal arrays: theory and applications*, Springer Science & Business Media, New York, 2012, pp. 317–339.
- [21] P. Dudek, FDM 3D printing technology in manufacturing composite elements, *Arch. Metall. Mater.* 58 (4) (2013) 1415–1418.
- [22] S. Singh, R. Singh, *Integration of fused deposition modeling and vapor Smoothing for biomedical applications, reference module in materials science and materials engineering*, Elsevier, 2017.
- [23] M. Somireddy, A. Czekanski, C.V. Singh, Development of constitutive material model of 3D printed structure via FDM, *Mater. Today Commun.* 15 (2018) 143–152.
- [24] Z. Qiu, C. Yao, K. Feng, Z. Li, P.K. Chu, Cryogenic deformation mechanism of CrMnFeCoNi high-entropy alloy fabricated by laser additive manufacturing process, *Int. J. Lightweight Mater. Manuf.* 1 (1) (2018) 33–39.
- [25] J. Lee, A. Huang, Fatigue analysis of FDM materials, *Rapid Prototyp. J.* 19 (4) (2013) 291–299.
- [26] X.L. Liao, W.F. Xu, Y.L. Wang, J. Bi, G.Y. Zhou, Effect of porous structure on mechanical properties of C/PLA/nano-HA composites scaffold, *Trans. Nonferrous Metals Soc. China* 19 (2009) s748–s751.
- [27] L. Wang, J. Kang, C. Sun, D. Li, Y. Cao, Z. Jin, Mapping porous microstructures to yield desired mechanical properties for application in 3D printed bone scaffolds and orthopaedic implants, *Mater. Des.* 133 (2017) 62–68.